R. H. Dean[1] *and J. W. Hutchinson*[2]

Quasi-Static Steady Crack Growth in Small-Scale Yielding

REFERENCES: Dean, R. H. and Hutchinson, J. W., "**Quasi-Static Steady Crack Growth in Small-Scale Yielding,**" *Fracture Mechanics: Twelfth Conference, ASTM STP 700,* American Society for Testing and Materials, 1980, pp. 383-405.

ABSTRACT: A numerical analysis of quasi-static, steady-state crack growth under small-scale yielding conditions has been carried out for antiplane shear (Mode III) and plane strain, Mode I. In addition to results for an elastic-perfectly plastic solid, the study includes results relating to the influence of strain hardening on stable crack growth. Limited results based on a corner theory of plasticity give some indication of the extent to which stable crack growth predictions are sensitive to the type of plasticity theory used.

KEY WORDS: elastic-plastic crack growth, plane strain, Mode III, steady crack growth, small scale yielding, fractures (materials), crack propagation

Crack-tip plasticity is primarily responsible for the phenomenon of stable crack growth in metals under monotonically increasing load or displacement conditions. As the crack advances, a material element just above or below the plane of the crack experiences a distinctly nonproportional history of straining; that is, the relative proportions of the strain components vary strongly as the tip passes beneath or above the element. By contrast, a material element in the vicinity of a stationary crack experiences predominantly proportional plastic loading. An elastic-plastic solid offers considerably more resistance to nonproportional strain histories than to proportional ones, and this is the main source of stable crack growth. In small-scale yielding the strain at a given distance from the tip in the plastic zone is larger in the stationary problem than it is in the steady growth problem at the same value of the stress intensity factor K.

[1] Assistant professor of engineering mechanics, Department of Engineering Mechanics, Ohio State University, Columbus, Ohio 43210.

[2] Professor of applied mechanics, Division of Applied Sciences, Harvard University, Cambridge, Mass. 02138.

For a stationary crack in an elastic-perfectly plastic solid the strains increase as $1/r$ as the distance from the tip r is diminished. For a growing crack the strain singularity is the weaker, $\ln(1/r)$, as has been discussed by Rice [*1*][3]. The character of the singular behavior at the tip of a growing crack in a hardening material has been found for linear strain hardening by Amazigo and Hutchinson [*2*]; but for more realistic hardening characterizations, such as power-law hardening, the near-tip singularity fields have remained elusive.

In carrying out a numerical analysis of a growing crack starting from its stationary state it is necessary to specify a near-tip fracture criterion or some relation between the crack advance and the applied load or displacement parameter. Various techniques have been proposed for such analyses and some of the most recent papers pursuing this approach are included in Ref *3*. As the crack advances, the increment in applied load or displacement needed to achieve a given increment of growth diminishes. In small-scale yielding the crack approaches nominally steady-state growth conditions, with an unchanging stress intensity factor K, following a crack advance which is one or two times the plastic zone size associated with the steady-state K. It is this steady-state problem which is studied in the present paper. Small-scale yielding is invoked, and all traces of the transient growth period are assumed to have been left far behind the current crack tip. As seen in Fig. 1, the crack is semi-infinite with a wake of residual plastic strains trailing behind the advancing tip. The formulation and solution of the steady-state problem does not require the specification of a fracture criterion. Instead, K plays the role of a scaling parameter to which all stress and strain quantities are related. Studies of the steady-state problem in Mode III have been published by Chitaley and McClintock [*4*] and by Andersson [*5*], who also considers plane stress in Mode I.

The present paper begins by reexamining the Mode III problem. Some

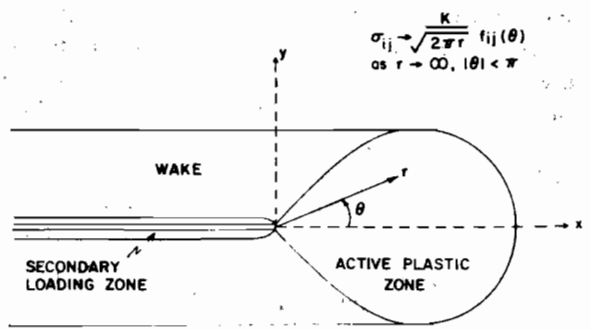

FIG. 1—*Steady-state crack growth in small-scale yielding.*

[3]The italic numbers in brackets refer to the list of references appended to this paper.

modification of the Chitaley-McClintock solution for elastic-perfectly plastic materials is noted. The effects of strain hardening and of corner development on the yield surface are also taken into account, and an attempt is made to assess their influence on the level of K required for steady-state growth compared to the K needed to cause crack growth initiation. The second part of the paper deals with plane-strain crack growth in Mode I for hardening and nonhardening materials. Contact with the recent results of Rice and Sorensen [*6*] and Rice, Drugan, and Sham [*7*] is made in the steady-state limit.

Numerical Analysis of Steady Growth

In the small-scale yielding limit, the elastic singularity field is imposed as the far field limit via a semi-infinite crack as depicted in Fig. 1. Thus, as $r \to \infty$

$$\sigma_{ij} = \frac{K}{\sqrt{2\pi r}} f_{ij}(\theta) \tag{1}$$

where the θ-variations depend on the symmetry of the field with respect to the crack plane $y = 0$. The material is elastically isotropic and the standard definition of K is employed throughout. It is imagined that the crack has grown from the left in Fig. 1 under steady-state conditions at constant K. The stress and strain fields around the moving crack tip will appear unchanging to an observer moving with the tip. At any fixed material point an increment of any quantity such as the stress is given by

$$\dot{\sigma}_{ij} = -\dot{a}\, \partial\sigma_{ij}/\partial x \tag{2}$$

where $\dot{a}$ is the increment of crack advance.

It is convenient to nondimensionalize the equations. In Mode III the dimensionless quantities are

$$\bar{w} = \frac{G\tau_0 w}{K^2} \qquad \bar{r} = \left(\frac{\tau_0}{K}\right)^2 r$$
$$\bar{\gamma}_\alpha = G\gamma_\alpha/\tau_0 \qquad \bar{\tau}_\alpha = \tau_\alpha/\tau_0 \tag{3}$$

where

τ_0 = the yield stress in shear,
G = the elastic shear modulus,
w = the displacement in the z-direction,
$\tau_\alpha = \sigma_{\alpha 3}$, and $\gamma_\alpha = 2\epsilon_{\alpha 3}$.

The dimensionless problem is independent of K. A similar nondimensionalization will be used for the Mode I problem.

A displacement-based finite element method is employed in the analysis. In a standard vector notation, the variational equation of equilibrium is

$$\int \sigma^T \delta\epsilon \, dA = \int \mathbf{F}^T \delta\mathbf{u} \, ds \tag{4}$$

where dA is an area element and tractions $\mathbf{F}$ from Eq 1 are applied on a circuit with line element, ds, far from the tip. The strains and displacements are given in terms of the nodal displacements $\mathbf{U}$ by

$$\epsilon = \mathbf{BU} \quad \text{and} \quad \mathbf{u} = \mathbf{RU} \tag{5}$$

where small-strain theory is assumed. The stresses are given by

$$\sigma = \mathbf{D}^e(\epsilon - \epsilon^p) \tag{6}$$

where $\mathbf{D}^e$ is the elastic constitutive matrix and ϵ^p is the plastic strain. With $\mathbf{K}^e = \int \mathbf{B}^T\mathbf{D}^e\mathbf{B} \, dA$ as the elastic stiffness matrix, the nodal displacements must satisfy

$$\mathbf{K}^e\mathbf{U} = \int \mathbf{R}^T\mathbf{F} \, ds + \int \mathbf{B}^T\mathbf{D}^e\epsilon^p \, dA \tag{7}$$

The iterative procedure for solving Eq 7 is as follows:

1. Given the estimate of ϵ^p from the $i - 1^{\text{th}}$ iteration, use it in Eq 7 to compute the i^{th} estimate of $\mathbf{U}$, $\mathbf{U}^{(i)}$.
2. Compute $\gamma^{(i)}$ everywhere from $\mathbf{U}^{(i)}$.
3. Compute $\sigma^{(i)}$ in the elastic region ahead of the plastic zone using $\sigma^{(i)} = \mathbf{D}^e\epsilon^{(i)}$.
4. Using the steady-state relation

$$\partial\sigma_{ij}/\partial x = D^{ep}_{ijkl} \, \partial\epsilon_{kl}/\partial x \tag{8}$$

integrate in the negative x-direction through the elastic-plastic elements to obtain $\sigma^{(i)}$, where $\partial\epsilon_{kl}/\partial x$ is obtained by taking appropriate differences in $\epsilon^{(i)}$ between elements. Here $\mathbf{D}^{ep}$ is the instantaneous tangent moduli from the elastic-plastic constitutive relation. In the active plastic zone where the yield condition is currently met, $\mathbf{D}^{ep}$ is the matrix of the loading moduli, while $\mathbf{D}^{ep}$ takes on elastic values where the stress falls within the yield surface. A technique similar to that in Rice and Tracey [8] was used to compute the normal to the yield surface for the current iteration.

5. Compute the i^{th} estimate of the plastic strain everywhere using

$$\epsilon^p = \epsilon - (\mathbf{D}^e)^{-1}\sigma$$

6. Repeat Steps 1 through 5 until convergence is achieved.

The basic element used was the constant strain triangle. The finite element mesh, shown schematically in Fig. 2, is composed of triangles and quadrilaterals, the latter being formed from four triangles with the center node condensed out. A mesh consisting of 1609 degrees of freedom before condensation was used in the Mode III calculations, while twice that number was used in the Mode I calculations. In Mode III the size of the smallest quadrilateral element was 0.4 percent of the distance to the elastic-plastic boundary directly ahead of the crack on the x-axis, while the corresponding figure in plane strain Mode I was 3 percent or about 1 percent of the height of the plastic zone in the y-direction.

A form of parameter tracking was used to facilitate convergence of the iteration scheme. The elastic solution ($\epsilon^p = 0$) was used to produce the first iteration for a high hardening case. When this case had converged the hardening parameter (either the tangent modulus for the linear straining hardening or the hardening exponent for power hardening) was decreased and the distribution of ϵ^p in the previous case was used to start the new iteration. The elastic-perfectly plastic cases required the most iterations to achieve satisfactory convergence and 50 to 100 iterations were used. The elastic stiffness matrix $\mathbf{K}^e$ in Eq 7 remained unchanged during all the computations, and therefore was formed and decomposed only during the initial elastic solution.

Steady Growth in Mode III

Elastic-Perfectly Plastic Material Behavior

Results for the elastic-perfectly plastic case will be discussed first to show the relationship with the previous work on this problem by Chitaley and

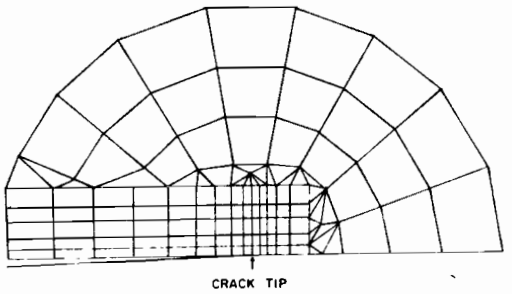

FIG. 2—*Coarse representation of finite element grid.*

McClintock [4]. In Mode III the Mises and Tresca yield conditions both reduce to

$$\tau_x^2 + \tau_y^2 = \tau_0^2 \tag{9}$$

Prandtl-Reuss equations (J_2 flow theory) were assumed in conjunction with Eq 9.

The plastic zone is shown in Fig. 3 using the nondimensional coordinates as axes. For comparison, the plastic zone for the corresponding stationary problem in small-scale yielding is also shown. The elastic-plastic boundary of the stationary problem is circular and extends a distance $\pi^{-1}(K/\tau_0)^2$ ahead of the tip. The position of the elastic-plastic boundary for the growing crack was interpolated from the numerical results. Its distance ahead of the tip at the plane of the crack is about 10 percent greater than for the stationary problem at the same K, that is

$$r_p \cong 0.36(K/\tau_0)^2 \tag{10}$$

The zone computed by Chitaley and McClintock extended about 5 percent beyond the stationary zone ahead of the crack. However, the main difference between the zone of Fig. 3 and that computed by Chitaley and McClintock is that their active zone was confined between two radial lines emanating from the tip at about 20 deg on either side of the plane of the crack. The active zone of Fig. 3 extends to almost ±60 deg from the plane of the crack. The numerical scheme employed by Chitaley and McClintock appears to have involved the built-in assumption that the slip lines (that is, the straight lines along which the resolved shear stress equals τ_0) all pass

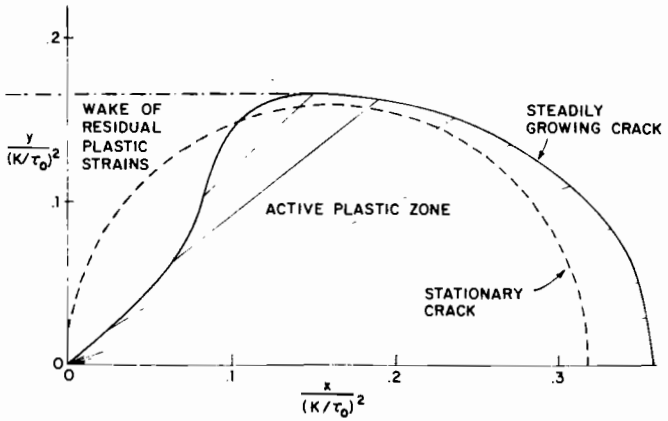

FIG. 3—*Active plastic zone for steady-state crack growth in an elastic-perfectly plastic material in Mode III small-scale yielding.*

through the crack tip. In other words, they assumed the plastic zone could be characterized by a centered fan of slip lines. Numerical results presented here indicate that this is not the case as can be seen from the lines of maximum shear stress shown in Fig. 3. For lines making an angle less than about 20 deg with $y = 0$ it does appear that the lines focus at the tip, but for angles greater than this the lines would intersect the plane of the crack behind the tip if extended out of the active plastic zone. The greater the angle with the x-axis, the further back the point of intersection.

In light of these findings we have reexamined the asymptotic analysis of Chitaley and McClintock for the stress field at the crack tip in Mode III. In particular, the possibility of a wedge shaped sector of nonfocused slip lines was considered, as suggested by the above results, in addition to the sectors containing a centered fan and elastic unloading considered by Chitaley and McClintock. The authors were unable to find an asymptotic stress field different from that of Chitaley and McClintock which was consistent with the requirement that the plastic work rate of the near-tip stresses be everywhere positive. Even though the smallest quadrilateral element at the tip used in calculating the results of Fig. 3 was less than 0.4 percent of the size of the active plastic zone, there is no evidence in the results to suggest that the asymptotic stress field, with its ±20 deg focused fan and elastic unloading outside the fan, is approached. Assuming that the asymptotic field of Chitaley and McClintock is correct, it would appear that it is attained only at distances that must be less than 1 percent of the plastic zone size.

The strain ahead of the tip on the x-axis can be obtained by integrating the slip line equations with the result for $r \leq r_p$

$$\gamma_y = \gamma_0\left[1 + \ln(r_p/r) + \frac{1}{2}\ln^2(r_p/r)\right] \tag{11}$$

where $\gamma_0 = \tau_0/G$ is the yield strain in shear. Since the estimate of r_p (Eq 10) is only about 5 percent larger than that of Chitaley and McClintock, the authors' findings for the strain ahead of the crack are in fairly close agreement with theirs. To give some indication of the accuracy of the present numerical results for the strains, one notes that the computed results for γ_y agreed closely with Eq 11 for values of γ_y/γ_0 less than 15, corresponding to r/r_p greater than 0.01, as will be seen in a subsequent figure.

Curves of the crack opening displacement, $\delta = w(x, y = 0^+) - w(x, y = 0^-)$, behind the tip are shown in Fig. 4. Included in that plot for comparison purposes are curves for the stationary problem for an elastic material and for an elastic-perfectly plastic material; namely, the curve for the growing crack in an elastic-perfectly plastic material and

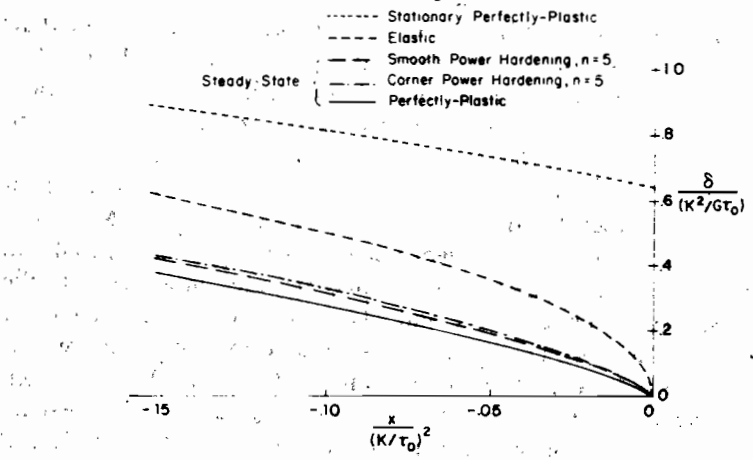

FIG. 4—*Comparison of crack opening (shearing) displacements in Mode III for stationary and growing cracks.*

curves for two hardening materials, which will be discussed below. In steady growth in an elastic-perfectly plastic material, the crack opening displacement goes to zero like $r \ln (1/r)$ as $x = -r$ goes to zero. A numerical fit to the finite element results for δ, which is displayed in Fig. 5, gives

$$\frac{\delta G \tau_0}{K^2} = 0.83 \frac{r\tau_0^2}{K^2} \ln \left(\frac{2.17K^2}{r\tau_0^2} \right) \tag{12}$$

Linear Strain Hardening

With

$$\tau = (\tau_x^2 + \tau_y^2)^{1/2} \tag{13}$$

the incremental flow law for plastic loading of a linear strain hardening material in antiplane shear is

$$G_t \dot{\gamma}_\beta = \alpha \dot{\tau}_\beta + (1 - \alpha)\tau_\beta \dot{\tau}/\tau \qquad \text{for } \dot{\tau} > 0 \tag{14}$$

where G_t is the constant tangent modulus of the shear stress-strain curve and $\alpha = G_t/G$. For elastic unloading or within the yield surface, $\dot{\tau}_\beta = G\dot{\gamma}_\beta$.

Amazigo and Hutchinson [*2*] have determined the crack-tip singularity fields for steady-state growth in the linear hardening material (Eq 14). Asymptotically as $r \to 0$, they find

$$\tau_\beta \sim r^s \bar{\tau}_\beta(\theta), \qquad \dot{\gamma}_\beta \sim r^{s-1}\dot{\bar{\gamma}}(\theta), \qquad w \sim r^{s+1}\bar{w}(\theta) \tag{15}$$

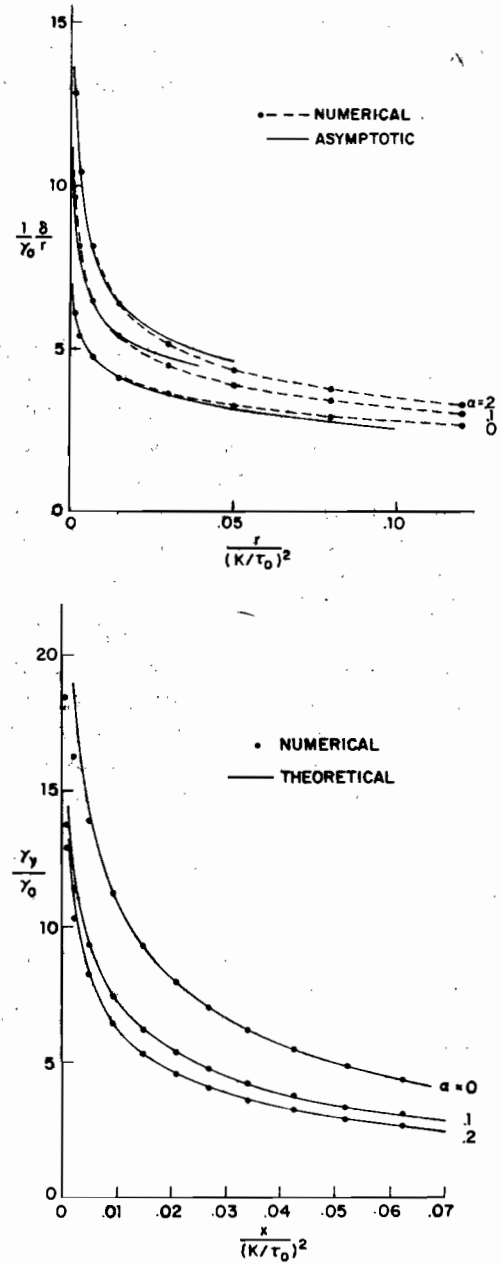

FIG. 5—*Comparison of numerical results with theoretical results chosen to give best fit as discussed in the text for Mode III.*

where s and the θ-variations depend on α. With $\bar{r}$ as the nondimensional radial distance defined in Eq 3, Eq 15 implies that the strain just ahead of the crack on $y = 0$ and the crack opening displacement just behind the crack should be of the form

$$\gamma_y/\gamma_0 = c_1\bar{r}^s + c_2 \tag{16}$$

$$\frac{\delta G\tau_0}{K^2} = c_3\bar{r}^{s+1} \tag{17}$$

where c_1, c_2, and c_3 are undetermined constants. (It is possible that there are additional singular terms, of lower order than r^s, which should appear in Eq 16. These have not been determined and are not taken into account here.) The coefficients in Eqs 16 and 17 were chosen to fit to the finite element results. Solid line curves in Fig. 5 are from Eqs 16 and 17 with the coefficient values shown in Table 1. The finite element values are shown as solid dots. The s-values in Table 1 are taken from Ref *2*, Table 1. Included in Fig. 5 are the elastic-perfectly plastic finite element results, together with curves from Eqs 11 and 12.

The strain hardening parameter α has relatively little influence on the location of the elastic-plastic boundary as can be seen in Fig. 6. The angular extent of the active zone near the tip on either side of $\theta = 0$ increases as α increases in approximate agreement with the predictions of the asymptotic analysis of Ref *2*. The present numerical results reveal a very small reversed zone of plastic yielding in the wake behind the tip. But this secondary zone extended less than 2 percent of the height of the plastic zone above and below the crack flank. The effect of this secondary zone, which was taken into account in Ref *4* but not in Ref *2*, appears to play a negligible role in Mode III.

These results can be used to obtain some insight into the role of strain hardening as it affects stable crack growth in small-scale yielding. First, consider a strain-based fracture criterion similar to the one proposed by McClintock and Irwin [*9*] where crack growth can initiate or continue if ahead of the crack in the plastic zone

$$\gamma_y = \gamma_c \quad \text{at} \quad r = r_c \tag{18}$$

TABLE 1—*Coefficient values.*

α	s	c_1	c_2	c_3
0.1	−0.207	5.25	−6.35	2.30
0.2	−0.277	2.61	−3.06	2.02

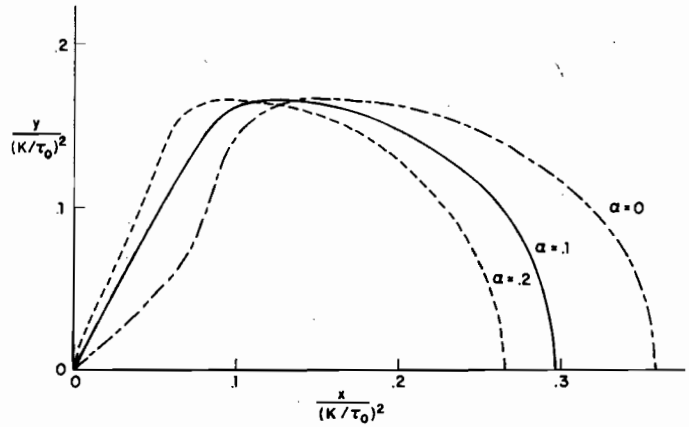

FIG. 6—*Effect of linear hardening parameter α on active plastic zone shape in Mode III.*

Reviewing quickly for the elastic-perfectly plastic case ($\alpha = 0$), one uses the strain ahead of the crack in the stationary problem

$$\gamma_y/\gamma_0 = r_p^s/r \quad \text{where} \quad r_p^s = \pi^{-1}(K/\tau_0)^2 \tag{19}$$

together with γ_y from Eq 11 for the steadily growing crack and the growth criterion from Eq 18 to determine the ratio of K_{ss} needed to drive the crack in steady-state to K_c needed to initiate growth. If one approximates r_p in Eqs 10 and 11 by r_p^s in Eq 19, as McClintock and Irwin did, one obtains

$$(K_{ss}/K_c)^2 = (\gamma_0/\gamma_c)\exp\left[\sqrt{2(\gamma_c/\gamma_0) - 1} - 1\right] \tag{20}$$

showing that K_{ss}/K_c may be very large if the "fracture strain," γ_c, is many times the yield strain, γ_0.

For the linear hardening material the strain ahead of the crack in the plastic zone of the small-scale yielding stationary problem can be shown from Ref *10* to satisfy

$$\bar{r} = \frac{1}{\pi(1-\alpha)}\left[\frac{\gamma_0}{\gamma_y} + \frac{\alpha}{1-\alpha}\ln\left(\frac{\alpha\gamma_y}{\alpha\gamma_y + (1-\alpha)\gamma_0}\right)\right] \tag{21}$$

where $\bar{r}$ is again given by Eq 3. For $\alpha \to 0$, Eq 21 yields Eq 19; and for $\alpha \neq 0$, Eq 21 gives $\gamma_y/\gamma_0 \to (2\pi\alpha\bar{r})^{-1/2}$ as $\bar{r} \to 0$. The full relation (Eq 21) was used in the following calculation. Using Eq 21 for the stationary problem and Eq 11 or 16 for the steady-state problem, together with the imposed growth criterion (Eq 18), the ratio K_{ss}/K_c for $\alpha = 0$, 0.1 and 0.2

was calculated. The ratio, which depends only on γ_c/γ_0, is plotted in Fig. 7. Note that the curve for the elastic-perfectly plastic case ($\alpha = 0$) is not exactly as indicated by Eq 20, since in Fig. 7 the more accurate result for r_p from Eq 10 has been used. Although linear hardening does not provide a very realistic representation of most stress-strain behavior, the trend with increasing hardening in Fig. 7 is clearly a decrease in the potential for stable crack growth. The exponential-type dependence of K_{ss}/K_c on large γ_c/γ_0, as typified for the zero hardening case by Eq 20, results from the weak logarithmic strain distribution (Eq 11) ahead of the growing crack. Hardening leads to a more robust singularity in the strains (see Eq 16 and Table 1) and consequently to smaller values of K_{ss}/K_c at large γ_c/γ_0.

An alternative growth criterion, which will be used later in the Mode I analysis, is based on a critical crack opening displacement (COD) a given distance behind the crack, as has been employed by Rice and Sorensen [6] in their Mode I analysis, that is

$$\delta = \delta_c \quad \text{at} \quad r = r_c \tag{22}$$

For the stationary problem in Mode III small-scale yielding [10]

$$\bar{r} = \begin{cases} -\dfrac{\alpha}{1-\alpha}\left\{\dfrac{1}{2}\bar{\delta} + \dfrac{1}{(1-\alpha)\pi}\ln\left[1 - \dfrac{\pi}{2}(1-\alpha)\bar{\delta}\right]\right\} & \bar{\delta} < \dfrac{2}{\pi} \\ \dfrac{\pi}{8}\bar{\delta}^2 - \dfrac{\alpha}{\pi(1-\alpha)^2}(1-\alpha+\ln\alpha) - \dfrac{1}{2\pi} & \bar{\delta} \geq \dfrac{2}{\pi} \end{cases} \tag{23}$$

where $\bar{\delta} = \bar{w}(r, \pi) - \bar{w}(r, -\pi)$ and $\bar{r}$ and $\bar{w}$ are given in Eq 3. The growth criterion (Eq 22) was used in conjunction with the numerical data for the growing crack and for the stationary crack (Eq 23) to generate K_{ss}/K_c as a function of $\delta_c/(\gamma_0 r_c)$ for $\alpha = 0$, 0.1 and 0.2. The results are shown in Fig. 8. Again one sees a decrease in the potential for stable crack growth with an increase in hardening.

Power Hardening with Smooth and Cornered Yield Surfaces

A limited study was made for a power hardening material that deforms in monotonic shearing according to

$$\begin{aligned} \gamma/\gamma_0 &= \tau/\tau_0 \qquad \tau \leq \tau_0 \\ &= (\tau/\tau_0)^n \qquad \tau > \tau_0 \end{aligned} \tag{24}$$

The asymptotic form of the singularity fields is not known for a growing

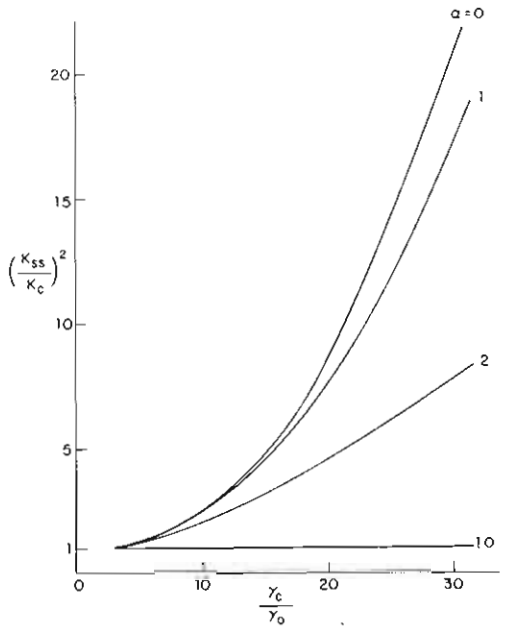

FIG. 7—*Dependence of* K_{ss}/K_c *on hardening in Mode III as predicted from a near-tip growth criterion based on attainment of a critical strain* γ_c *a distance* r_c *ahead of the tip.*

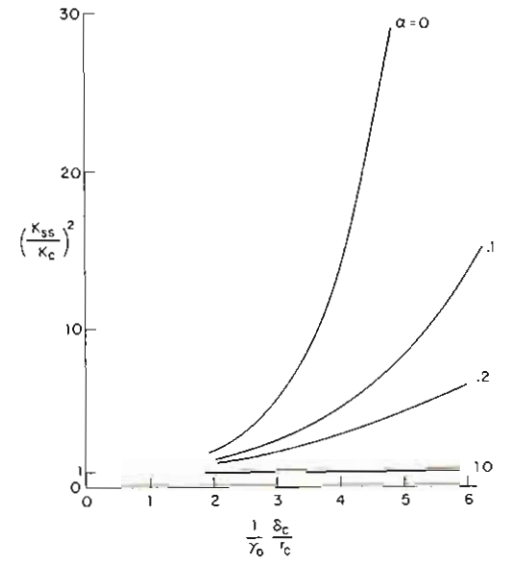

FIG. 8—*Dependence of* K_{ss}/K_c *on hardening in Mode III as predicted from a growth criterion based on attainment of a critical shearing displacement* δ_c *a distance* r_c *behind the tip.*

crack in a power law material, as has already been mentioned. Our main concern here will be to contrast the results from two different flow theories, both of which satisfy Eq 24 in pure shear. One employs the classical smooth isotropic hardening surface based on Eq 13 (that is, J_2 flow theory), and the other is a recently proposed [*11*] law, called J_2 corner theory, in which a corner develops on the yield surface at the loading point. Subsequent yield surfaces for the two theories in antiplane shear are shown in Fig. 9.

Plastic loading according to the classical J_2 flow theory requires

$$\dot{\gamma}_\alpha = G^{-1}\dot{\tau}_\alpha + (G_t^{-1} - G^{-1})\tau_\alpha \dot{\tau}/\tau \tag{25}$$

where G_t is the current tangent modulus whose dependence on τ is obtained from Eq 24.

The plastic strain-rate given by the second term in Eq 25 is constrained to lie along the normal to the yield surface. In a nonproportional stress history, such as that shown in Fig. 9 where the ratios of the stress components change, the stiffness associated with the component of stress increment, which is tangent to the yield surface, is necessarily the elastic value. Crack growth inherently involves strongly nonproportional stressing in material elements lying above and below the plane of the crack, as mentioned in the beginning of this paper. Isotropic hardening based on the smooth Mises yield surface tends to overestimate the resistance of an elastic-plastic material to nonproportional deformation. A corner theory of plasticity, by contrast, probably underestimates somewhat the resistance to nonproportional deformation, although perhaps not significantly. Thus, a comparison of results based on the two theories may give some indication as to whether the extensive stable crack growth predicted by classical flow theory (as indicated by the large values of K_{ss}/K_c) is realistic.

Full details of J_2 corner theory are given in the paper by Christoffersen and Hutchinson [*11*]. In their notation, the angle between the axis of the corner (see Fig. 9) and the stress-rate is given by

$$\cos\beta = \tau_\alpha \dot{\tau}_\alpha/(\tau\sqrt{\dot{\tau}_\mu \dot{\tau}_\mu}) \tag{26}$$

The total strain-rate is given by $\dot{\gamma}_\alpha = \partial W/\partial \dot{\tau}_\alpha$ where W is the stress-rate potential defined by

$$W = \frac{1}{2G} Q(\beta)\dot{\tau}_\alpha \dot{\tau}_\alpha \tag{27}$$

The strain-rate is

$$G\dot{\gamma}_\alpha = \left(Q + \frac{1}{2} Q' \operatorname{cotan}\beta\right)\dot{\tau}_\alpha - \frac{1}{2} Q' (\sin\beta \cos\beta)^{-1}\tau_\alpha \dot{\tau}/\tau \tag{28}$$

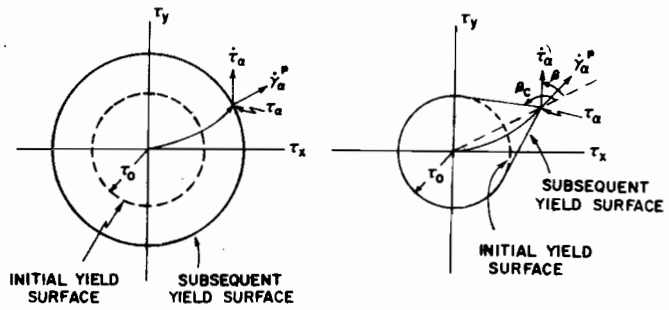

FIG. 9—*Two yield surfaces employed in the Mode III power hardening calculations.*

where $Q' = dQ/d\beta$. The function $Q(\beta)$ provides a smooth transition from a proportional loading increment ($\beta = 0$) to elastic unloading for $\beta \geq \beta_c$. For proportional loading the predictions of Eq 25 and 28 are identical, and for nearly proportional loading the strain-rates from Eq 28 coincide with the predictions of the J_2 deformation theory of plasticity. The function $Q(\beta)$ used in the calculations reported below is specified by the function $g(\phi)$ defined in Ref *11*, Eq 2.46 (with $m = 3$ and $\theta_0 = 0$).

The active plastic zones for the smooth theory and corner theory with $n = 5$ are shown in Fig. 10. Ahead of the crack the plastic boundaries are essentially coincident. The corner theory unloading boundary trails the isotropic hardening unloading boundary. The corner theory active zone is somewhat larger than that for isotropic hardening, reflecting the diminished resistance of the corner theory material to nonproportional stress histories.

Curves of COD behind the tip for the classical flow theory and the corner

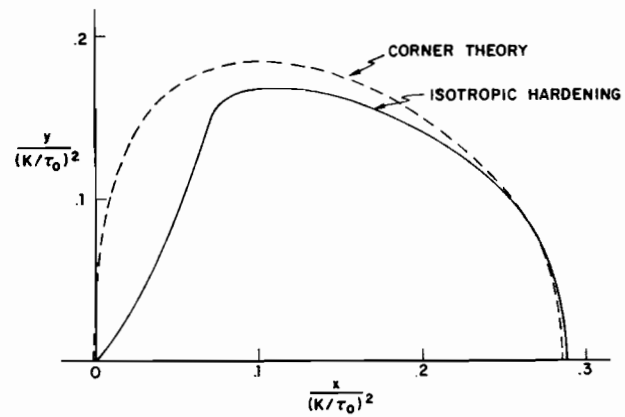

FIG. 10—*Comparison of active plastic zones in Mode III for power hardening* (n = 5) *for two yield surface characterizations.*

theory for $n = 5$ are included in Fig. 4. Over the portion of the plastic zone in which the present results are accurate (that is, to within about 1 percent of the plastic zone size from the tip), there is rather little difference in the results for the two theories. The COD, a given distance behind the tip, is slightly larger for the corner theory material than for the smooth yield surface material. This small difference again reflects the lowered resistance that the corner theory material offers to nonproportional plastic deformation.

The strain ahead of the crack from the two theories is shown in Fig. 11. Here again the difference is small but now the strain from the smooth yield surface solid is slightly larger than the other, at least for strains less than 15 γ_0 for which the authors' results are accurate. This somewhat surprising interchange can be rationalized by noting that the deformation on the line ahead of the crack is exactly proportional ($\tau_x = 0$), while nonproportional deformation takes place above and below the plane of the crack. Examination of the numerical results indicates that the standard flow theory solid tends to concentrate the straining in the region ahead of the crack, compared to the corner theory solid. Although the effect is not large, the corner theory solid shows relatively more straining above and below the line of the crack, consistent with what one would expect and consistent with its slightly larger opening displacement.

Our study of the influence of reduced resistance to nonproportional flow

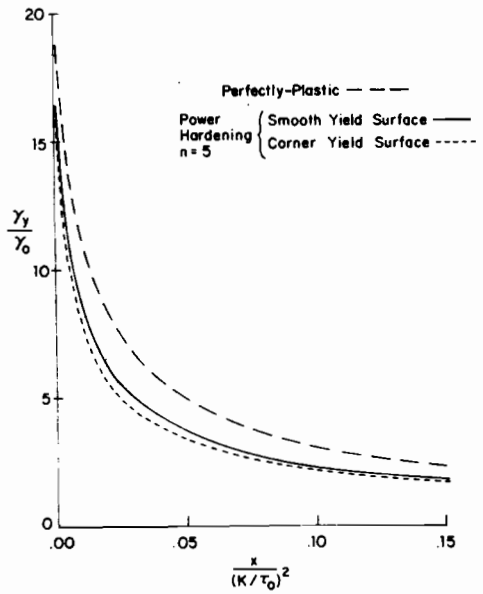

FIG. 11—*Strain ahead of crack in Mode III for power hardening theories and comparison with elastic-perfectly plastic distribution.*

as modeled by the corner theory has not been sufficiently extensive to warrant the apparent conclusion that the effect is not very large. It is possible that larger discrepancies will emerge closer to the tip at higher strain levels. One also notes that use of the corner theory results, as opposed to the standard flow theory results, with the critical strain criterion (Eq 18) would yield slightly higher estimates of K_{ss}/K_c. On the other hand, use of the corner theory results for the opening displacement with Eq 22 would give slightly lower estimates of this ratio, at least over the range considered here. Nevertheless, it does appear that the influence of strain hardening may be more significant than the corner effect.

Steady Growth in Plane Strain Mode I

In the plane strain study a piecewise-power law material was assumed whose uniaxial stress-strain curve is given by

$$\begin{aligned} \epsilon/\epsilon_0 &= \sigma/\sigma_0 \qquad \sigma < \sigma_0 \\ &= (\sigma/\sigma_0)^n \qquad \sigma > \sigma_0 \end{aligned} \tag{29}$$

where

σ_0 = the uniaxial yield stress,
$\epsilon_0 = \sigma_0/E$ = the yield strain, and
E = Young's Modulus.

The classical incremental theory (J_2 flow theory) was used to generalize Eq 29 to multiaxial states. This theory assumes isotropic hardening based on the Mises surface (that is, $J_2 = 1/2\ s_{ij}s_{ij}$ = constant, where s_{ij} is the stress deviator). The material was taken to be elastically isotropic with Poisson's ratio, ν. Included in Eq 29 for $n \to \infty$ is elastic-perfectly plastic behavior.

Amazigo and Hutchinson [*2*] obtained singularity fields for the plane strain, Mode I problem for linear strain hardening. However, they neglected the effect of reversed plastic loading along the flank of the crack behind the tip. The present numerical results indicate that substantial reversed loading occurs in plane strain, and therefore its omission in Ref *2* is likely to render those results inaccurate. For this reason no attempt was made to use the linear hardening material in the present plane strain study.

The elastic-plastic boundary of the active plastic zone is shown in Fig. 12 for the elastic-perfectly plastic material ($n = \infty$) and for $n = 3$ and 10. Poisson's ratio was taken to be $\nu = 0.3$ in all cases. The zone in which "reversed" plastic flow occurs, trails behind the tip as shown with a width that is approximately 15 percent of the vertical extent of the plastic zone for $n = 10$ and ∞.

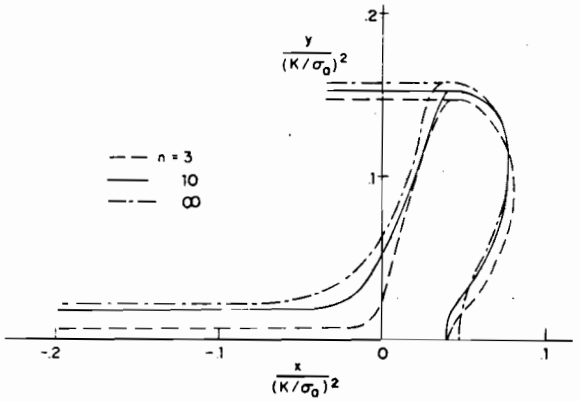

FIG. 12—*Active plastic zone in plane strain Mode I small-scale yielding for two levels of power hardening and elastic-perfectly plastic behavior.*

Stresses near the tip as determined from the finite element results for the elastic-perfectly plastic material are shown in Fig. 13. The numerical results are compared with the asymptotic near-tip stress field recently determined by Rice et al [7]. These new asymptotic stresses differ only by about 1 percent from the stresses of the Prandtl field, except in the neighborhood of $\theta = 135$ deg, where the differences are on the order of 10 percent. The main difference between the new asymptotic field and the Prandtl field is

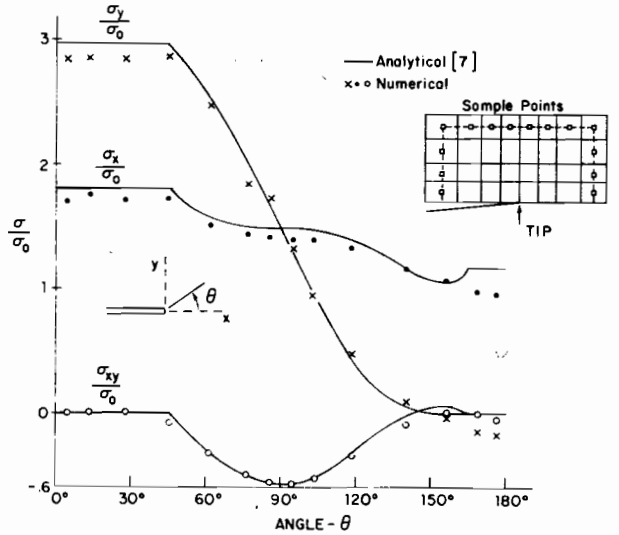

FIG. 13—*Comparison of the near-tip numerical stress results with asymptotic field of Ref 7 for plane strain Mode I.*

the presence of a wedge of elastic unloading extending from approximately $\theta = 115$ deg to $\theta = 163$ deg, whereas yield is satisfied for all θ in the Prandtl field. There is no evidence in the authors' numerical results of elastic unloading near the tip. As can be seen in Fig. 12, the active plastic zone appears to fully surround the tip. It is quite likely that the mesh refinement used in the present calculations is not sufficient to reveal the wedge shaped unloading region. In Mode III it was noted that the mesh used indicated a substantially smaller wedge of elastic unloading near the tip than that predicted by the Chitaley-McClintock asymptotic field. In plane strain, the mesh used in this analysis is relatively coarser (the smallest quadrilateral element is about 3 percent of the distance to the elastic plastic boundary ahead of the crack) and this may explain the authors' failure to observe any elastic unloading near the tip.

Curves of the nondimensional COD behind the crack for the steady growth problem are shown in Figs. 14*a* and *b*. The linear elastic curve ($n = 1$) is shown in Fig. 14*a*. The numerical values from the finite element calculations for the elastic-perfectly plastic case ($n = \infty$) are shown as solid dots in Fig. 14*b*. As the tip is approached the opening displacement goes to zero as

$$\delta = \beta \frac{\sigma_0}{E} r \ln\left(\frac{eR}{r}\right) \tag{30}$$

where, following the notation of Rice and Sorensen [6], β is a numerical constant (with no relation to the angle β used in the corner theory), $e = 2.7183$ and $R = c(K/\sigma_0)^2$ where c is another numerical constant. The best least-square fit of Eq 30 to the four computed values of δ nearest the tip (see Fig. 14*b*) gives

$$\beta = 4.28 \quad \text{and} \quad c = 0.71 \tag{31}$$

The analysis of Rice et al [7], which employs the asymptotic near-tip field mentioned above, gives the theoretical value $\beta = 5.08$. Fixing β at 5.08 and choosing c to give a best least-square fit of the same four values of δ, one finds

$$\beta = 5.08 \quad \text{and} \quad c = 0.28 \tag{32}$$

This latter estimate of c is in reasonable agreement with the value obtained in Ref 7 from a fit of numerical data for the transient growth of a crack. Curves from Eq 30, using Eq 31 and 32, are shown in Fig. 14*b*. There is relatively little difference between the two curves for $x/(K/\sigma_0)^2$ in the range -0.001 to -0.02.

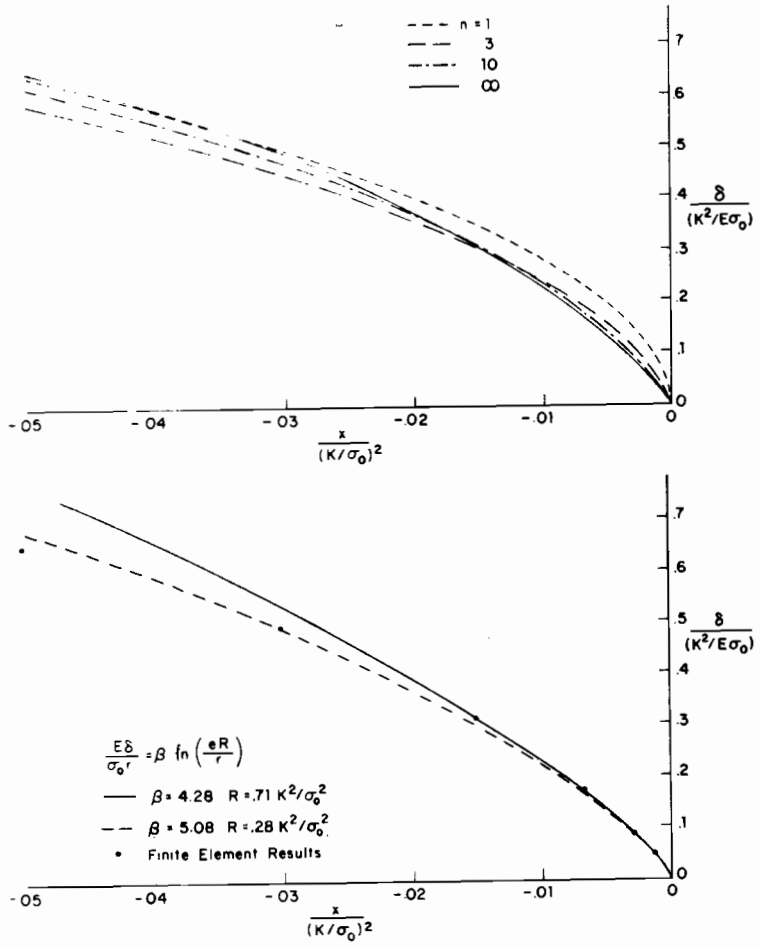

FIG. 14—*Crack opening displacement in plane strain Mode I* (a) *effect of hardening, and* (b) *numerical values for elastic perfectly plastic case* (n = ∞) *and comparison with asymptotic formula.*

The results for δ for $n = 3$, 10 and ∞ have been replotted as $\delta/(\epsilon_0 r)$, where $\epsilon_0 = \sigma_0/E$, as a function of $r/(K/\sigma_0)^2$ in Fig. 15. It is in this form that the results are most convenient for predicting K_{ss}/K_c from a near-tip fracture criterion based on a critical δ.

Following Rice and Sorensen [*6*], and also Ref *7*, one again adopts the near-tip criterion (Eq 22) for initiation and continuation of crack growth. For a given value of $\delta_c/(\epsilon_0 r_c)$ and n, the value of $r_c/(K_{ss}/\sigma_0)^2$ for steady-state growth can be read off the abscissa of Fig. 15. The value of $r_c/(K_c/\sigma_0)^2$ for initiation of growth can be read from the corresponding curve for the stationary problem. These two values supply the ratio $(K_{ss}/K_c)^2$ for a given

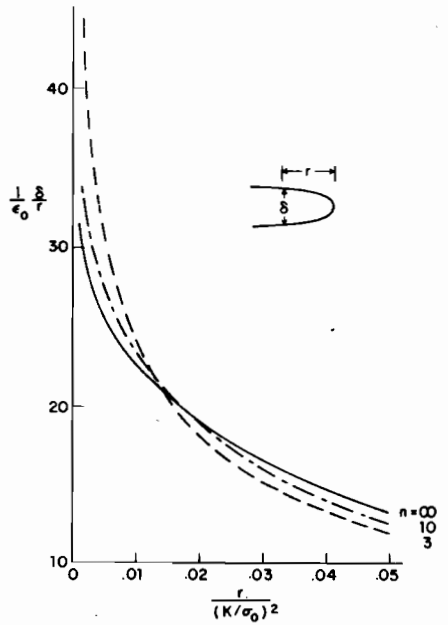

FIG. 15—*Normalized crack opening displacement in plane strain Mode I.*

pair $\delta_c/(\epsilon_0 r_c)$ and n. Curves obtained in this manner are plotted in Fig. 16 for $n = 3$, 10 and ∞. For the stationary problem the authors derived curves of $\delta/(\epsilon_0 r)$ versus $r/(K/\sigma_0)^2$ from Ref *12* for $n = 3$ and ∞ and from Ref *6* for $n = 10$. However, the n-dependence of the stationary solution for δ plays a relatively minor role in determining the influence of hardening on the variation of K_{ss}/K_c with $\delta_c/(\epsilon_0 r_c)$ in Fig. 16. Primarily, the influence of hardening on the curves in Fig. 16 is due to the dependence of the steady growth solution of Fig. 15 on the hardening index n.

The strong dependence of K_{ss}/K_c on hardening is qualitatively similar to what was found in Mode III for linear hardening. The curves in Fig. 16 were not extrapolated to values of $\delta_c/(\epsilon_0 r_c)$ beyond about 32, corresponding to the limit to which the numerical results are felt to be accurate. Rice and Sorensen [*6*] suggest that values of $\delta_c/(\epsilon_0 r_c)$ larger than 100 may be appropriate for certain intermediate strength pressure vessel steels with unusually high tear resistance. Then, values of K_{ss}/K_c will be enormous for light to moderate strain hardening ($10 \leq n \leq \infty$, say) as can be seen from the trends of Fig. 16. But it is also clear from these trends that the elastic-perfectly plastic result for a given $\delta_c/(\epsilon_0 r_c)$ appears to significantly overestimate the potential for stable crack growth in a hardening material. It seems reasonable to assume that the same conclusion holds for the entire transient growth process. That is, one expects that the normalized resistance

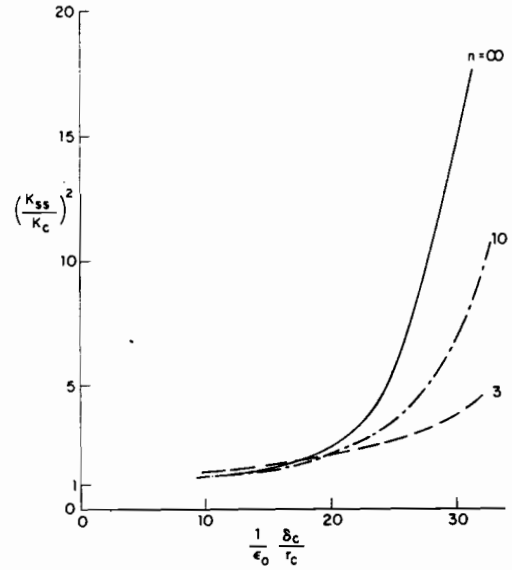

FIG. 16—*Effect of hardening on* K_{ss}/K_c *in plane strain Mode I as predicted by a criterion based on the attainment of a critical opening displacement* δ_c *a distance* r_c *behind the current tip.*

curve in small-scale yielding (that is, K_R/K_c as a function of Δa), as predicted using a near-tip fracture criterion such as the one employed here, will be strongly influenced by small to moderate amounts of hardening. Predictions for elastic-perfectly plastic solids will tend to be unconservative when strain hardening is present.

Acknowledgments

We are indebted to D. M. Parks and his colleague P. S. Lam for making available for comparison purposes some of their results for the Mode III problem, which were obtained using a similar numerical method to that employed here. We also acknowledge receipt of an early version of Ref *7* from J. R. Rice and helpful discussions with him in connection with the asymptotic near-tip fields. This work was supported in part by the National Science Foundation under Grant NSF-ENG78-10756, and by the Division of Applied Sciences, Harvard University. In addition, R. H. Dean acknowledges support in the initial stages of the work from a National Science Foundation Graduate Fellowship.

References

[*1*] Rice, J. R. in *Mechanics and Mechanisms of Crack Growth*, British Steel Corp., 1973.
[*2*] Amazigo, J. C. and Hutchinson, J. W., *Journal of the Mechanics and Physics of Solids*, Vol. 25, 1977, pp. 81–97.

[*3*] *Elastic-Plastic Fracture, ASTM STP 668*, American Society for Testing and Materials, 1979.
[*4*] Chitaley, A. D. and McClintock, F. A., *Journal of the Mechanics and Physics of Solids*, Vol. 19, 1971, pp. 147–163.
[*5*] Andersson, H., *Journal of the Mechanics and Physics of Solids*, Vol. 22, 1974, pp. 285–308.
[*6*] Rice, J. R. and Sorensen, E. P., *Journal of the Mechanics and Physics of Solids*, Vol. 26, 1978, pp. 163–186.
[*7*] Rice, J. R., Drugan, W. J., and Sham, T. L., "Elastic Plastic Analysis of Growing Cracks," Technical Report No. 65, Division of Engineering, Brown University, May 1979.
[*8*] Rice, J. R. and Tracey, D. M. in *Numerical and Computer Methods in Structural Mechanics*, Academic Press, New York, 1973, pp. 585–623.
[*9*] McClintock, F. and Irwin, G. R. in *Fracture Toughness Testing and Its Applications, ASTM STP 381*, American Society for Testing and Materials, 1965, pp. 84–113.
[*10*] Rice, J. R., *Journal of Applied Mechanics*, Vol. 34, 1967, pp. 287–298.
[*11*] Christoffersen, J. and Hutchinson, J. W., *Journal of the Mechanics and Physics of Solids*, Vol. 27, 1979, pp. 465–487.
[*12*] Shih, C. F., Andrews, W. R., German, M. D., VanStone, R. H., and Wilkinson, J. P. D., "Methodology for Plastic Fracture," Report No. SRD-78-116, Combined Seventh and Eighth Quarterly Report by General Electric Company to Electric Power Research Institute, Inc., July 1978.